Journal of Power Sources 233 (2013) 28–33

Contents lists available at SciVerse ScienceDirect

Journal of Power Sources

journal homepage: www.elsevier.com/locate/jpowsour

Effect of electrolyte temperature on the pseudo-capacitive behavior of manganese oxide in N-butyl-N-methylpyrrolidinium–dicyanamide ionic liquid

Ming-Tsung Lee [a,*], Wen-Ta Tsai [a], Hui-Fang Cheng [b], I-Wen Sun [b], Jeng-Kuei Chang [c]

[a] Department of Materials Science and Engineering, 1 University Road, National Cheng Kung University, Tainan, Taiwan
[b] Department of Chemistry, National Cheng Kung University, Tainan, Taiwan
[c] Institute of Materials Science and Engineering, National Central University, Taoyuan, Taiwan

HIGHLIGHTS

► Good pseudo-capacitive performance of Mn oxide was found in BMP–DCA IL at 80 °C.
► Specific capacitance of 93 F g^{-1} is obtained at 80 °C, which is 50% higher than those obtained at 30 °C.
► The Mn oxide has a high energy and power densities in BMP–DCA IL at high temperature.

ARTICLE INFO

Article history:
Received 16 August 2012
Received in revised form
27 November 2012
Accepted 16 January 2013
Available online 26 January 2013

Keywords:
Pseudo-capacitance
Ionic liquid
Temperature effect
Electrolyte

ABSTRACT

The electrochemical behavior of anodically deposited Mn oxide in N-butyl-N-methylpyrrolidinium–dicyanamide (BMP–DCA) ionic liquid (IL) at various temperatures (30–80 °C) is investigated. Cyclic voltammetry (CV) is used to evaluate the electrochemical performance of the Mn oxide. Surface morphology of the deposited oxide after charging/discharging is examined by scanning electron microscopy (SEM). The experimental data show that the Mn oxide electrode exhibits good pseudo-capacitance performance even at 80 °C. In the ionic liquid studied, the specific capacitance increases with increasing BMP–DCA IL temperature. A specific capacitance of 93 F g^{-1} in a potential window of 3 V is obtained at 80 °C, which is about 50% higher than that obtained at 30 °C. The experimental results also show that the capacitance-retained ratio of the oxide electrode increases with increasing temperature at a high potential sweep rate. Furthermore, the capacitance decline about 40% after 500 repeated charging/discharging cycles in BMP–DCA IL at 80 °C is observed, which is better than that measured in an aqueous electrolyte.

1. Introduction

Supercapacitors are charge-storage devices that have a greater power density and longer cycle life compared to those of batteries, and a higher energy density compared to that of conventional capacitors [1–3]. Accordingly, they have been developed for a range of applications, such as in hybrid electric vehicles, peak power sources, backup power storage, medical electronics, and military missile systems. Supercapacitors can be classified based on their operating mechanisms into two categories: (1) double-layer capacitors, which are based on non-faradaic charge separation at the electrode/electrolyte interface; and (2) pseudocapacitors, which are based on the faradic redox reaction of electroactive materials. Manganese oxide is considered a favorable electrode material for use in supercapacitors [4–9] due to its satisfactory electrochemical performance, its natural abundance, and environmental compatibility.

The charge storage (pseudo-capacitive) mechanism of Mn oxide in an aqueous electrolyte has been proposed as follows [10,11]:

$$MnO_2 + n\,C^+ + n\,e^- \leftrightarrow MnO_{2-n}(OC)_n \quad (1)$$

$$(MnO_2)_{surface} + C^+ + e^- \leftrightarrow (MnO_2\ ^-C^+)_{surface} \quad (2)$$

where C^+ denotes the protons or alkali metal cations (Li^+, Na^+, K^+) in the electrolyte. Eq. (1) suggests that both protons and alkali cations are involved in the bulk redox process. And Eq. (2) proposed that the mechanism of the surface adsorption of electrolyte cations (C^+) on MnO_2

Among the constituent components of a supercapacitor, the electrolyte governs the overall performance. Due to the intrinsic characteristics of water decomposition, common aqueous electrolytes have narrow potential windows (typically ~ 1 V for three-

* Corresponding author. Tel.: +886 6 2757575x62942; fax: +886 6 2754395.
E-mail address: roy_tsung@hotmail.com (M.-T. Lee).

0378-7753/$ – see front matter © 2013 Elsevier B.V. All rights reserved.
http://dx.doi.org/10.1016/j.jpowsour.2013.01.104

electrode system) [12,13], which limits the available capacitor cell voltage. Since both the energy density and power density of a supercapacitor change with the square of the cell voltage, an electrolyte with a large stable potential window is desirable. In order to solve the narrow potential windows in aqueous solution, a promising way to increase cell voltage is development of asymmetric supercapacitors. Asymmetric supercapacitors can make use of the different potential windows of the two electrodes to increase the maximum operation voltage in the cell system, resulting in an enhanced specific capacitance and significantly improved energy density. Recently, to obtain higher energy density, considerable research efforts have been devoted to the various asymmetric capacitor systems, such as activated carbon AC//MnO_2 [14–17], AC//V_2O_5 [18], carbon nanotube (CNT)//MnO_2 [19], AC//$K_{0.27}MnO_2 \cdot 0.6H_2O$, AC//$NaMnO_2$ [20,21], AC//Graphene/MnO_2 [22].

In addition, the organic solvent as the electrolyte has a wide potential window also considered. Although organic solvents have relatively larger electrochemical windows of stability, they produce serious health and safety problems as volatile, flammable, and sometimes toxic. Finding a more suitable electrolyte to optimize the energy storage performance of supercapacitors is of great importance. Ionic liquids (ILs) have wide potential windows ; they can thus provide a large cell voltage, which benefits both the energy density and power density of a supercapacitor. The non-volatility and nonflammability of ILs make them safer than organic solvent electrolytes [23,24]. We have previously [25–29] demonstrated that manganese oxide electrodes show good pseudo-capacitive characteristics in dicyanamide (DCA)-based ILs at ambient temperature. The great thermal stability of ILs allows a capacitor to be reliably operated at elevated temperature. Therefore, the effect of temperature on the material properties and capacitive behavior of manganese oxide in an IL is investigated in this study.

2. Experimental procedure

Aprotic N-butyl-N-methylpyrrolidinium–dicyanamide (BMP–DCA) IL was prepared and purified following a previously published method [26]. The IL was washed with acetone and dichloromethane sequentially, filtrated, and then vacuum-dried at 393 K. The water content of the IL, measured with a Karl Fisher titrator, was below than 100 ppm.

Mn oxide was anodically deposited from 0.25 M $Mn(CH_3COO)_2$ aqueous plating solution at room temperature [25]. A three-electrode electrochemical system was employed. A 1 cm × 1 cm Ni coupon working electrode (with a thickness of 120 μm and an exposed area of 1 cm^2) was etched in 2 M HCl solution at 80 °C, washed with pure water in an ultrasonic bath, and used after drying. A platinum sheet and a saturated calomel electrode (SCE) were assembled as the counter electrode and reference electrode, respectively. The electrodeposition was performed at a constant potential of 0.8 V (vs. SCE) to give a total passed charge of 0.4 Coulombs cm^{-2}. The typical mass per area of the deposited oxide, measured using a microbalance with an accuracy of 0.01 mg, was approximately 0.3 mg cm^{-2} (with a thickness of about 1 μm). The surface morphology of the oxide electrode was examined with a scanning electron microscope (SEM, Hitachi SU-1500). The crystal structure of the Mn oxide was analyzed by glancing angle X-ray diffraction (GAXRD). The patterns were recorded on a Rigaku D/MAX-2500 diffractometer with a glancing incident angle of 1°. Cu Kα radiation with a wavelength of 1.5418 A was used as the X-ray source. A Netzsch STA 409 analyzer was used to perform simultaneous thermogravimetric and differential thermal (TG/DT) analyses of the BMP–DCA IL. The IL was heated from 25 to 1500 °C at a rate of 10 °C min^{-1} under a flowing N_2 atmosphere. The N_2 flow rate was 20 mL min^{-1}.

The electrochemical properties of the Mn oxide electrode in BMP–DCA IL were characterized by cyclic voltammetry (CV) and chronopotentiometry (CP) at various temperatures (30–80 °C) in a nitrogen-purified glove box (Vacuum Atmospheres Co.), where both the moisture content and oxygen content were maintained below 1 ppm. A Pt wire placed in a fritted-glass tube containing butylmethylpyrrolidinium–bis (trifluoromethylsulfony) imide IL

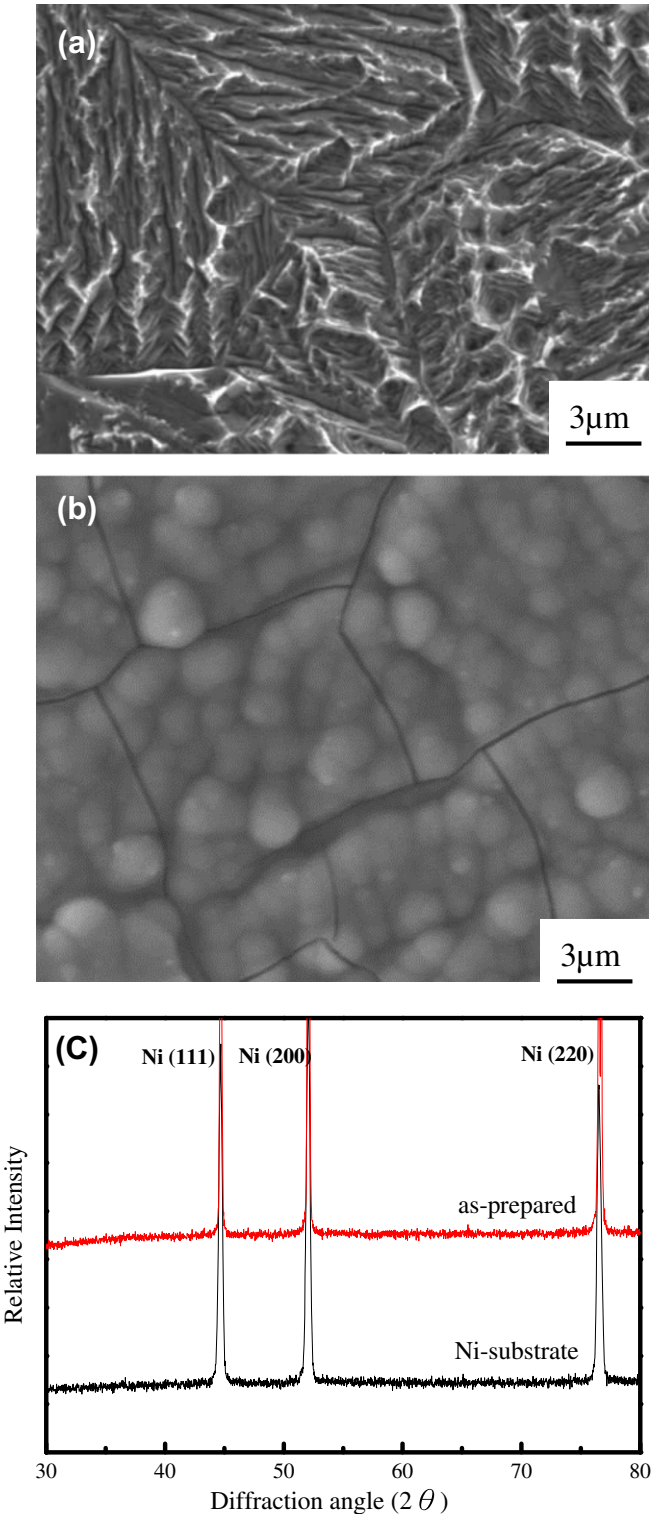

Fig. 1. SEM micrographs of (a) Ni substrate and (b) as-prepared Mn oxide electrode. (c) XRD patterns of as-prepared Mn oxide electrode.

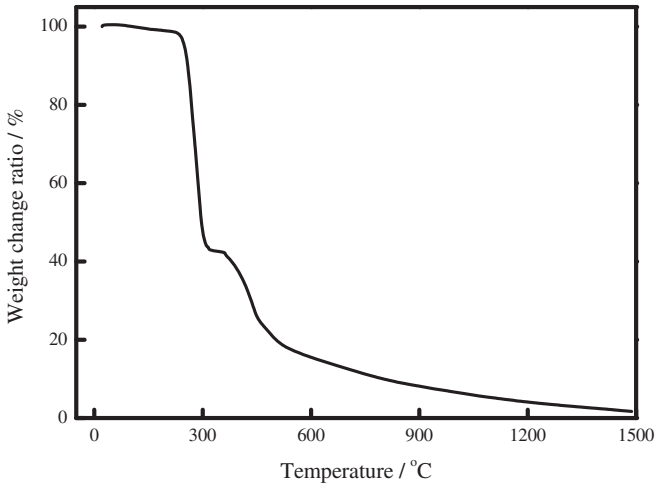

Fig. 2. TGA plot of BMP–DCA IL measured at a heating rate of 10 °C min^{-1} in an N_2 atmosphere.

was used as the quasi-reference electrode (showing a potential of +1.25 V vs. SCE). The counter electrode was a spiral Pt wire, which was directly immersed in the bulk BMP–DCA IL. The applied potential and current were regulated using an AUTOLAB potentiostat.

3. Results and discussion

3.1. Mn oxide electrode analyses

Fig. 1(a) shows an SEM micrograph of the etched Ni foil. The rough surface of the electrode substrate provided a high contact area and good adhesion with the deposited Mn oxide. Fig. 1(b) shows the surface morphology of the as-deposited Mn oxide electrode; a granular structure can be recognized. The cracks in the deposits can be attributed to the shrinkage of the deposited oxide during drying and/or vacuuming. It was also found that the electrode surface was flattened due to the oxide coverage. The crystal structure of the deposited Mn oxide was analyzed using GAXRD ; the results are shown in Fig. 1(c). The GAXRD pattern of the Ni substrate is also shown in this figure. No diffraction signal attributed to the deposit was detected, indicating that the Mn oxide was amorphous in nature. These results are consistent with previous reports [25–28].

3.2. TG/DT analyses of BMP–DCA ILs

Fig. 2 shows a TGA plot of the BMP–DCA IL measured in an N_2 atmosphere. The weight changes as a function of temperature are demonstrated in this figure. An initially sharp weight loss of about 60% accrued at 300 °C, which was followed by a weight loss of about 30% in the temperature range of the 350–800 °C. According to literature reports [30,31] that the pyrrolidinium salt was decomposed at about 250 °C, while the dicyanamide anion had much greater stability. Therefore the first weight loss was decomposition of the BMP–DCA IL, the products containing the monoalkylated pyrroles, pyrrolidines cations and dicyanamide anion. The weight loss in the temperature range of 350–800 °C could be attributed to the decomposition of the pyrrolidines cations and dicyanamide anion (DCA^-) residue. N_2, NH_3, and CO_2 could possibly be formed from the decomposition of this IL. Beyond this temperature (800 °C), the IL weight was gradually decreased until 1500 °C. These results suggest that the BMP–DCA is thermally stable at temperatures below 200 °C.

3.3. Electrochemical characteristics

Fig. 3(a)–(c) show the electrochemical behavior of the Mn oxide electrode recorded in BMP–DCA IL at various temperatures

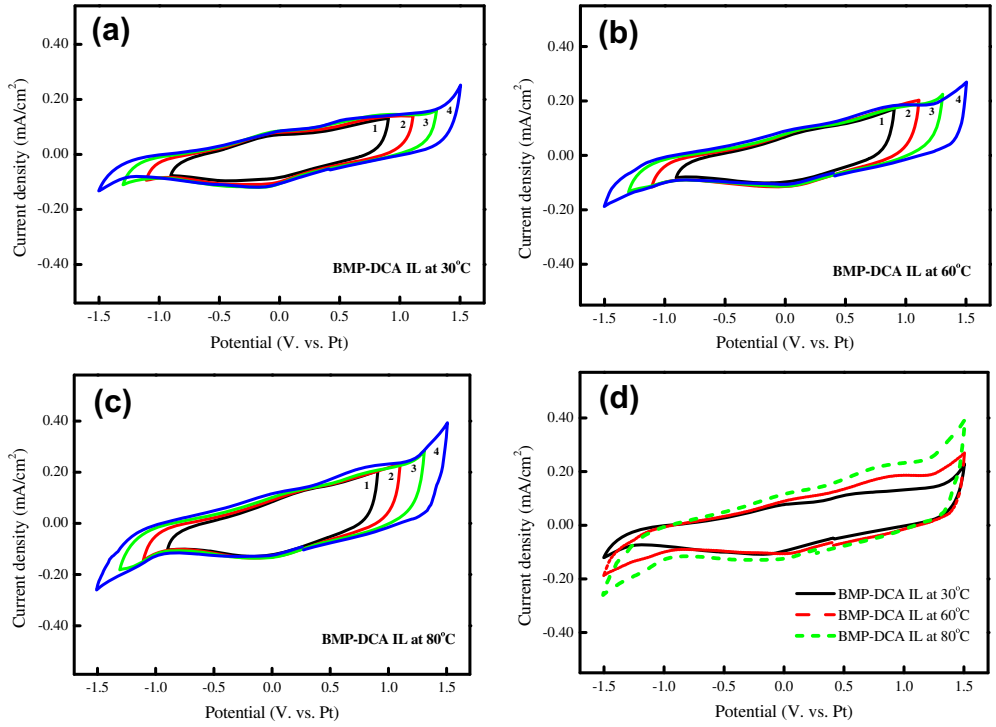

Fig. 3. Cyclic voltammograms of the Mn oxide electrode with upper and lower potential scanning limits of CV of (1) (0.9, −0.9), (2) (1.1, −1.1), (3) (1.3, −1.3), 4 (1.5, −1.5) in BMP–DCA IL at (a) 30 °C, (b) 60 °C, and (c) 80 °C. (d) Cyclic voltammograms of Mn oxide electrodes measured in BMP–DCA IL at various temperatures with a potential sweep rate of 5 mV s^{-1}.

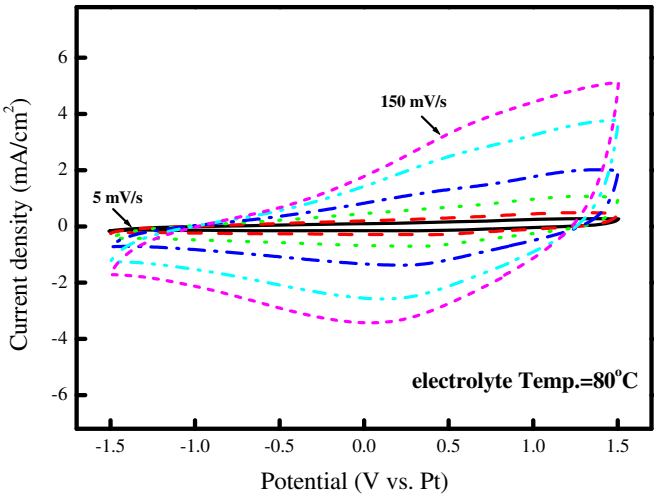

Fig. 4. Cyclic voltammograms of the Mn oxide electrode measured at potential sweep rates of 5, 10, 25, 50, 100, and 150 mV s^{-1} in BMP–DCA IL at 80 °C.

measured at different upper and lower potential scanning limits (−0.9–0.9 V_{pt}, −1.1–1.1 V_{pt}, −1.3–1.3 V_{pt} and 1.5 ∼ −1.5 V_{pt}, respectively) of CV, stretching from −1.5 V_{Pt} to +1.5 V_{Pt}, before irreversible cathodic and anodic reactions of Mn oxide occurred. Inside the potential region, the CV response current remained almost constant during forward and backward scans but it immediately affected its flow direction when the potential was reversed. The shapes of the CV curves are close to rectangular and symmetric in a potential range of approximately 3 V. The results demonstrate the excellent reversibility and good pseudo-capacitive behavior of the electrodes in BMP–DCA IL at temperatures up to 80 °C.

Moreover, the Mn oxide electrode at 80 °C maintained a wide operation potential window (3 V), indicating that this IL is promising for high-cell-voltage supercapacitors at high temperature. Fig. 3(d) compares the cyclic voltammograms of the Mn oxide measured in this IL in the potential range of 1.5 ∼ −1.5 V_{Pt} at various temperatures. The experimental results show that the enclosed area of the CV curve in this IL at high temperature is larger than that obtained at low temperature (i.e., 30 °C). It was worth noticing that, the CV curves have a general sloping behavior at high temperature may be attribute to (1) MnO_2 have passivation in the electrode or (2) the pseudocapacitive contribution of the Mn oxide in the high temperature is more than those in lower temperature. The specific capacitance (C) of Mn oxide can be calculated using the following equation:

$$C = Q_m / \triangle V \quad (3)$$

where Q_m is the specific voltammetric charge (based on weight) integrated from the CV curve and $\triangle$ V is the potential scanning range (3 V). The oxide specific capacitances measured in BMP–DCA at 30 °C, 60 °C, and 80 °C were 62 F g^{-1}, 75 F g^{-1}, and 93 F g^{-1}, respectively.

Table 2
Physical data of the BMP–DCA IL at various temperatures.

BMP–DCA IL Temp.	Conductivity (ms cm^{-1})	Viscosity (mPas)
30 °C	6.58	42.6
60 °C	11.08	18.5
80 °C	15.04	11.5

The cyclic voltammograms of the Mn oxide electrode measured in BMP–DCA IL at 80 °C with various potential sweep rates are shown in Fig. 4. It was found that the CV response current density progressively increased with increasing potential sweep rate, which is an ideal pseudocapacitive behavior, at 80 °C in BMP–DCA IL. These results indicate the high reactivity and great kinetic performance of the Mn oxide electrode at higher temperature in BMP–DCA IL. Table 1 lists the specific capacitances, calculated from the average of the anodic and cathodic charge measured at various CV scan rates, of the Mn oxide electrode in this IL at various temperatures. The Mn oxide at 80 °C in BMP–DCA IL had the highest specific capacitance at every CV scan rate. The superior performance of the oxide electrode at 80 °C in the IL can be attributed to the higher ionic conductivity and lower viscosity of the IL than those at lower temperatures, as shown in Table 2. Table 1 also shows that the capacitance declined with increasing potential scan rate. The internal iR drop of the electrode and the diffusion limitation of reactants and products near the electrode/electrolyte interface caused the capacitance decay at high potential scan rates. Furthermore, the capacitance-retained ratio of the Mn oxide was measured at various temperatures. At 80 °C, the specific capacitance of the oxide measured at 150 mV s^{-1} was about 61% of that at 5 mV s^{-1}. This capacitance-retained ratio is higher than that measured at 30 °C and can be attributed to increased ionic conductivity and lowered viscosity.

The electrochemical properties of the oxide electrode were also evaluated by CP, in which the applied charging and discharging current densities were both set at 0.1 mA cm^{-2}. Fig. 5(a) and 5(b) show the obtained chronopotentiogram of five sequential charging–discharging cycles in BMP–DCA IL at 30 °C and 80 °C, respectively. As can be seen from these figures, at both temperature, the charging and discharging branches are some curvature due to faradaic process. It is essentially close to linear and symmetric, indicating the ideal pseudocapacitive performance and good reversibility of Mn oxide in a potential range of 3 V, which is larger than that typically found for traditional aqueous electrolytes (∼1 V) [10,13]. From the CP data, the Mn oxide specific capacitance can be evaluated using:

$$C = I/(\triangle E/\triangle t)/w \quad (4)$$

where *I* is the applied current (0.1 mA), $\triangle$ E is the potential sweep range (3 V), $\triangle$ *t* is the total discharging time, and *w* is the mass of the oxide. The measured specific capacitances of Mn oxide from Fig. 5(a) and 5(b) are 68 F g^{-1} and 103 F g^{-1}, respectively, which are pretty close to the CV data.

To further evaluate the stability of Mn oxide in BMP–DCA IL at various temperatures, the cycle life of the oxide electrode was

Table 1
Specific capacitance of Mn oxide electrode at various temperatures in BMP–DCA IL.

BMP–DCA IL temperature	Specific capacitance (F g^{-1}) at indicated CV scan rate						Capacitance-retained ratio	After 500 cycles capacitance-retained ratio
	5 mV s^{-1}	10 mV s^{-1}	25 mV s^{-1}	50 mV s^{-1}	100 mV s^{-1}	150 mV s^{-1}		
30 °C	62	56	50	44	38	33	33/62 = 0.52	100%
60 °C	75	67	60	55	48	43	43/75 = 0.57	85%
80 °C	93	84	74	69	64	57	57/93 = 0.61	60%

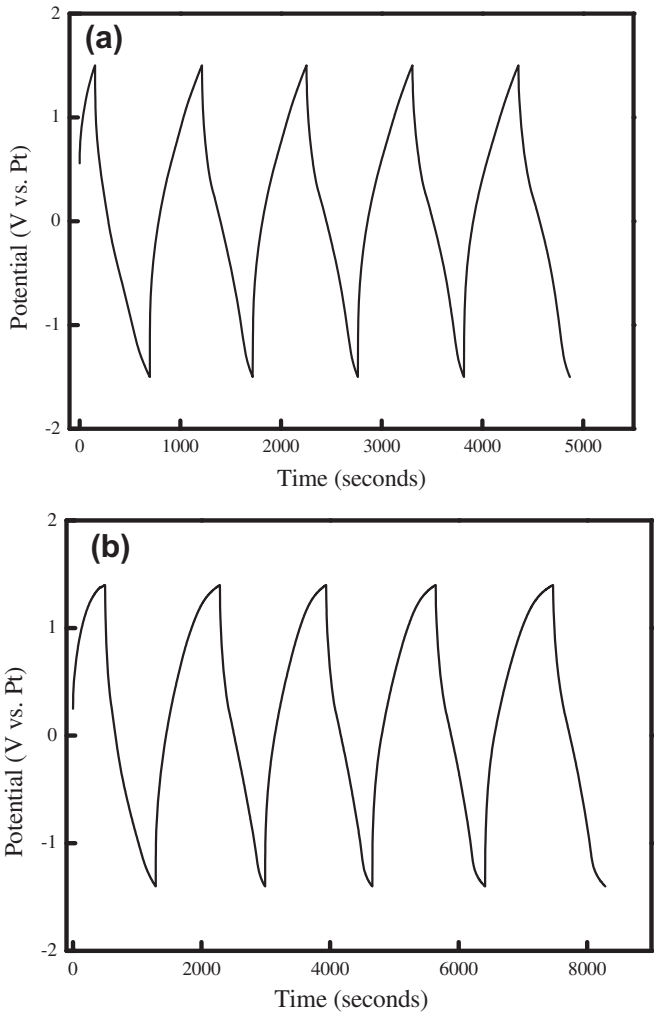

Fig. 5. Chronopotentiogram for 5 charge–discharge cycles of the Mn oxide electrode measured in BMP–DCA IL at (a) 30 °C and (b) 80 °C with an applied current density of ±0.1 mA cm^{-2}.

tested by repeating the CV scan at a rate of 20 mV s^{-1} for 500 cycles. Fig. 6 shows the variation of the capacitance-retained ratio with CV cycle number of the Mn oxide electrode measured in BMP–DCA IL at 80 °C, together with those measured in Na_2SO_4 aqueous solution. In our previous study and literature [27,32], no matter in BMP–DCA IL or in aqueous solution at the room temperature (about 30 °C), indicated that the Mn oxide electrode was good cycling stability performance. However, approximately 40% of the capacitance decayed at 80 °C after 500 CV cycles in BMP–DCA IL. The gradual increase of the measured capacitance during the first 50 cycles could be associated with the activation or wetting process of the oxide electrode in the IL. In Na_2SO_4 aqueous solution at 80 °C, the specific capacitance after 500 CV cycles decayed approximately 60%. Furthermore, as shown in this figure, the capacitance in Na_2SO_4 aqueous solution did not gradually increase during the first 50 CV cycles. These results suggest that the cycle life stability of Mn oxide in BMP–DCA at high temperature is better than that measured in aqueous electrolyte.

Fig. 7 shows SEM micrographs of the Mn oxide electrode after 500 CV cycles in BMP–DCA IL at 30 °C and 80 °C, respectively. At 30 °C in BMP–DCA IL, the granular surface morphology retained its integrity after CV cycling (Fig. 7(a)). Almost no structural change was observed, which assured the durability of the Mn oxide

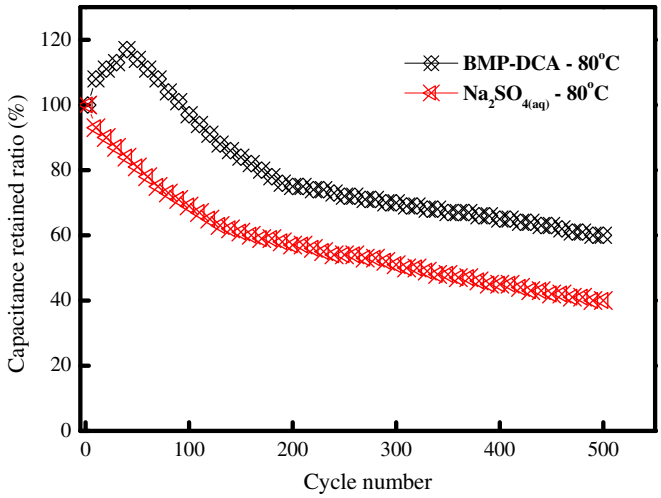

Fig. 6. Variation of the capacitance-retained ratio with CV cycle number of the Mn oxide electrode measured in BMP–DCA IL and Na_2SO_4 solution at 80 °C.

electrode in the testing electrolyte. However, serious detachment of the Mn oxide was clearly seen in IL (Fig. 7(b)) at 80 °C, similar to those obtained for Na_2SO_4 aqueous solution at 80 °C. Our previous studies [33,34] have indicated that capacitance decay occurred in

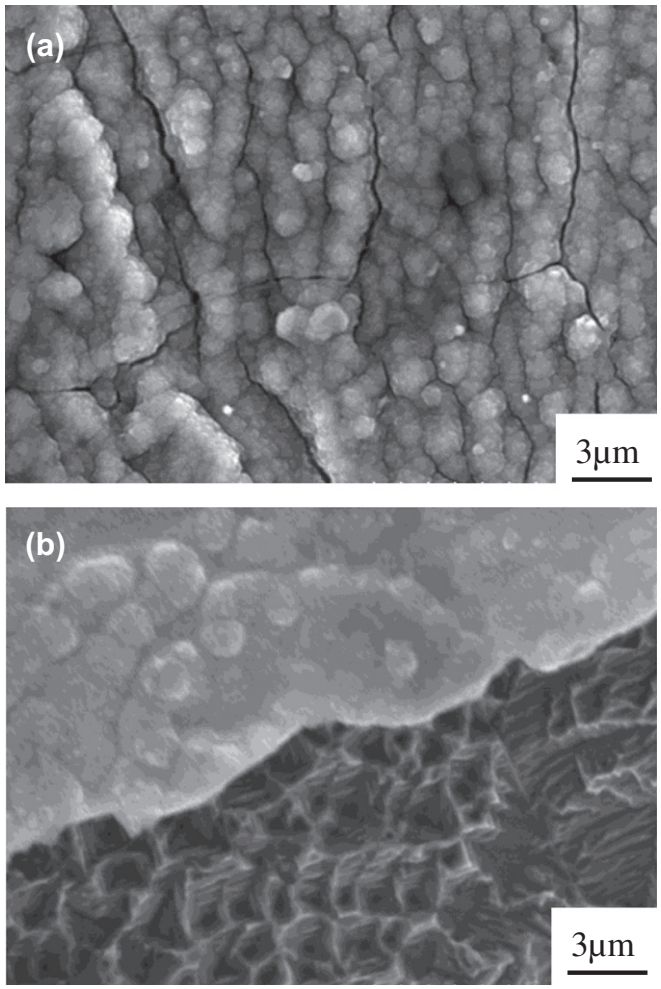

Fig. 7. SEM micrographs of the Mn oxide electrode after 500 CV cycles in BMP–DCA IL at (a) 30 °C and (b) 80 °C.

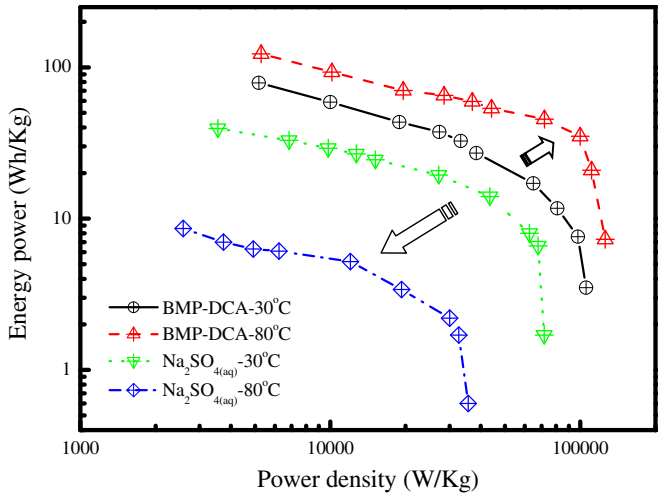

Fig. 8. Ragone plots for Mn oxide electrodes measured in BMP–DCA IL and Na_2SO_4 solution at 30 °C and 80 °C, respectively.

aqueous electrolyte at room temperature, after CV cycling mainly due to the detachment of the Mn oxide in water. Obviously, in high-temperature ILs or aqueous solutions, the Mn oxide detachment caused capacitance decay after CV cycling.

The Ragone plot represents the dependence of specific energy density on the specific power density. Fig. 8 shows the Ragone plots for the Mn oxide electrode measured in BMP–DCA IL and Na_2SO_4 aqueous solution at 30 °C and 80 °C, respectively. Specific energy density and the specific power density values were respectively calculated using:

$$E(Wh/kg) = [i(A) \times V(V) \times t(h)]/m(kg) \quad (5)$$

$$P(W/kg) = E(Wh/kg)/t(h) \quad (6)$$

where i is the discharge current, V is the voltage excluding the iR drop at the beginning of the discharge (Fig. 5), t is the time in hours, and m is the mass. The results indicate that the oxide in BMP–DCA IL had a higher specific energy density and specific power density than those obtained in Na_2SO_4 aqueous solution. In the BMP–DCA IL, the specific energy density and specific power density increased with increasing temperature. However, the reverse was observed in Na_2SO_4 aqueous solution. This could be attributed to the operation potential window being reduced to 0.6 V in Na_2SO_4 aqueous solution at high temperature, which resulted in decreased of energy density and power density.

4. Conclusion

Good pseudocapacitive performance of Mn oxide was found in an aprotic BMP–DCA IL electrolyte at high temperature (up to 80 °C), which maintained a wide operation potential window (3 V). The specific capacitance increased with increasing IL temperature. Specific capacitances of 93 F g^{-1} (CV measured, scan rate 5 V s^{-1}) and 103 F g^{-1} (CP measured) were obtained at 80 °C, which are about 50% higher than those obtained at 30 °C. Moreover, the capacitance-retained ratio of the Mn oxide electrode increased with increasing temperature at a high potential sweep rate. After 500 charging/discharging cycles in BMP–DCA IL at 80 °C, the specific capacitance of the oxide decayed by approximately 40%, which is attributed to the detachment of the Mn oxide in the IL. The applicable potential window of Mn oxide in BMP–DCA IL (3 V) is triple that found in traditional aqueous electrolytes and the specific capacitance at 80 °C is higher than that at room temperature. Therefore, both the energy and the power densities increase. Conversely, Mn oxide supercapacitor is unsuited to high-temperature aqueous electrolyte. This study demonstrated that the Mn oxide electrode has a high energy density and power density in BMP–DCA IL at high temperature, making it good for supercapacitor applications.

Acknowledgment

The authors would like to thank the National Science Council of the Republic of China (Taiwan) for financially supporting this research (under grants NSC 100-2221-E-006-239-MY3 and NSC 95-2221-E-006–192).

References

[1] B.E. Conway, Electrochemical Supercapacitors, Kluwer-Plenum, New York, 1999.
[2] P. Simon, Y. Gogotsi, Nat. Mater. 7 (2008) 845–854.
[3] G. Wang, L. Zhang, J. Zhang, Chem. Soc. Rev. 14 (2012) 797–828.
[4] C.C. Hu, T.W. Tsou, Electrochem. Commun. 4 (2002) 105–109.
[5] J.K. Chang, Y.L. Chen, W.T. Tsai, J. Power Sources 135 (2004) 344–353.
[6] A.E. Fischer, K.A. Pettigrew, D.R. Rolison, R.M. Stroud, J.W. Long, Nano Lett. 7 (2007) 281–286.
[7] J.K. Chang, C.H. Huang, W.T. Tsai, M.J. Deng, I.W. Sun, J. Power Sources 179 (2008) 435–440.
[8] O. Ghodbane, J.L. Pascal, F. Favier, ACS Appl. Mater. Interfaces 1 (2009) 1130–1139.
[9] W. Wei, X. Cui, W. Chen, D.G. Ivey, Chem. Soc. Rev. 40 (2011) 1697–1721.
[10] M. Toupin, T. Brousse, D. Bélanger, Chem. Mater. 16 (2004) 3184–3190.
[11] J.K. Chang, M.T. Lee, W.T. Tsai, J. Power Sources 166 (2007) 590–594.
[12] H.Y. Lee, J.B. Goodenough, J. Solid State Chem. 144 (1999) 220–223.
[13] M. Toupin, T. Brousse, D. Bélanger, Chem. Mater. 14 (2002) 3946–3952.
[14] V. Khomenko, E. Raymundo-Pinero, F. Beguin, J. Power Sources 153 (2006) 183–190.
[15] H.Q. Wang, Z.S. Li, Y.G. Huang, Q.Y. Li, X.Y. Wang, J. Mater. Chem. 20 (2010) 3883–3889.
[16] Q.T. Qu, P. Zhang, B. Wang, Y.H. Chen, S. Tian, Y.P. Wu, R. Holze, J. Phys. Chem. C 113 (2009) 14020–14027.
[17] T. Brousse, P.L. Taberna, O. Crosnier, R. Dugas, P. Guillemet, Y. Scudeller, Y. Zhou, F. Favier, D. Belanger, P. Simon, J. Power Sources 173 (2007) 633–641.
[18] Q.T. Qu, Y. Shi, L.L. Li, W.L. Guo, Y.P. Wu, H.P. Zhang, S.Y. Guan, R. Holze, Electrochem. Commun. 11((2009) 1325–1328.
[19] P.C. Chen, G.Z. Shen, Y. Shi, H.T. Chen, C.W. Zhou, ACS Nano 4 (2010) 4403–4411.
[20] W. Tang, Y.Y. Hou, X.J. Wang, Y. Bai, Y.S. Zhu, H. Sun, Y.B. Yue, Y.P. Wu, K. Zhu, R. Holze, J. Power Sources 197 (2012) 330–333.
[21] Q.T.i Qu, L. Li, S. Tian, W. Guo, Y.P. Wu, R. Holze, J. Power Sources 195 (2010) 2789–2794.
[22] Z. Fan, J. Yan, T. Wei, L. Zhi, G. Ning, T. Li, F. Wei, Adv. Funct. Mater. 21 (2011) 2366–2375.
[23] J.F. Huang, H. Luo, C. Liang, I.-W. Sun, G.A. Baker, S. Dai, J. Am. Chem. Soc. 127 (2005) 12784–12785.
[24] H. Ohno, Electrochemical Aspects of Ionic Liquids, John Wiley & Sons, Hoboken, NJ, 2008.
[25] J.K. Chang, M.T. Lee, C.W. Cheng, W.T. Tsai, M.J. Deng, I.-W. Sun, Electrochemical Solid State Lett. 12 (2009) A19–A22.
[26] J.K. Chang, M.T. Lee, W.T. Tsai, M.J. Deng, I.-W. Sun, Chem. Mater. 21 (2009) 2688–2695.
[27] J.K. Chang, M.T. Lee, C.W. Cheng, W.T. Tsai, M.J. Deng, I.-W. Sun, J. Mater. Chem. 19 (2009) 3732–3738.
[28] J.K. Chang, M.T. Lee, W.T. Tsai, M.J. Deng, H.F. Cheng, I.-W. Sun, Langmuir 25 (2009) 11955–11960.
[29] M.T. Lee, W.T. Tsai, M.J. Deng, H.F. Cheng, I.-W. Sun, J.K. Chang, J. Power Sources 195 (2010) 919–922.
[30] D.R. MacFarlane, S.A. Forsyth, J. Golding, G.B. Deacon, Green Chem. 4 (2002) 444–448.
[31] T.J. Wooster, K.M. Johanson, K.J. Fraser, D.R. MacFarlane, J.L. Scott, Green Chem. 8 (2006) 691–696.
[32] Q.T. Qu, Y. Shi, S. Tian, Y.H. Chen, Y.P. Wu, R. Holze, J. Power Sources 194 (2009) 1222–1225.
[33] M.T. Lee, J.K. Chang, W.T. Tsai, J. Electrochem. Soc. 154 (2007) A875–A881.
[34] J.K. Chang, M.T. Lee, C.H. Huang, W.T. Tsai, Mater. Chem. Phys. 108 (2008) 124–131.